Turkish Journal of Physics

http://journals.tubitak.gov.tr/physics/

Research Article

Turk J Phys
(2021) 45: 1 – 12
© TÜBİTAK
doi:10.3906/fiz-2010-5

Interactions between densely grafted molten polymer brushes: Scaling theories versus molecular simulations

Aykut ERBAŞ*
UNAM National Nanotechnology Research Center and Institute of Materials Science & Nanotechnology, Bilkent University, Ankara, Turkey

Received: 14.10.2020 • **Accepted/Published Online:** 12.01.2021 • **Final Version:** 27.02.2021

Abstract: Using molecular dynamics simulations and scaling arguments, we analyzed the interactions between two identical molten polymer brushes intermediately and strongly compressed towards each other at melt conditions. The width of the overlap region, in which monomers of the linear chains composing the two brushes interact, increases as the polymer-grafted surfaces are brought closer. If two-brush coated surfaces are as close as the characteristics size of the grafted chains, the overlap region is directly controlled by intersurface distance. At intermediate compression, the width of the overlap region scales with the end-to-end size of chain sections within the overlap region. This result is consistent with the scaling regimes in the literature. As the intersurface distance is decreased, the number fraction of chains (chains with their free ends in the overlap region) decreases with a power law. Our results could be useful for studies on tribological behavior of polymer-grafted surfaces as well as for the self-assembly of polymer coated colloids.

Key words: Polymer brushes, melt, molecular dynamics

1. Introduction

Polymer brushes are monolayers of stretched polymer chains. They form when polymers are grafted on flat or curved surfaces by at least one of their monomers via physical or chemical bonds (Figure 1) [1]. While polymer brushes have been a subject of active researh for more than 30 years, the recent progress in radical polymerization methods [2, 3] have made them essential components of advance materials with unconventional properties [5, 6]. Some of these technological applications include control of self-assembly of brush-coated colloidal particles [7, 8], surface coatings for biomedical implants [9], molecular sensors [10, 11], temperature sensitive surfaces [12], smart drugs [13], antibacterial surfaces [14], and responsive materials [15, 16], etc.

Structures reminiscent of polymer brushes are also often encountered in nature. Particularly, surface parts of tissues that have to come into physical contact with each other at relatively high speeds are covered with layers of high-molecular weight polymers [17]. For example, the brush-like mucin layers that cover the inner parts of the eyelids and retinal surfaces function to prevent erosion that occurs during blinking [18, 19]. The cartilage tissue, which is located at the joining ends of the bones and prevents bone wear, also resembles polymer brushes [20, 21]. In general, brush-like structures are thought to function as protective layers minimizing the damage and wear during the relative movements of biological tissues.

One key point for above mentioned brush-based systems, whether they are biological or synthetic in

*Correspondence: aykut.erbas@unam.bilkent.edu.tr

nature, is that these brush-coated surfaces interact with each other by their grafted chains. Ultimately, the strength of these molecular-level interactions determines all macroscopic properties of the corresponding systems (i.e. whether brush-coated colloids would form aggregates, or the frictional forces between two brush-coated surfaces would be reduced by grafted chains). Thus, inevitably, in order to further advance in nanotechnological fields and design bioinspired systems, the interactions between the chains of brush-coated surfaces must be understood at the molecular scale.

The first pioneering study on polymer-grafted surface dates back to the Alexander–de Gennes (AG) model [22, 23]. In the AG model, the height of a brushlayer scales linearly with the polymerization degree of the polymers, N, predicting highly strecthed chains. The AG model assumes that all the grafted chains have identical heights, thus, the concentration profile of the chemical monomers in the direction perpendicular to the surface is a step function. Consequently, when two such brushes are brought to physical contact, no overlap occurs between the two brushes. Later studies corrected this model by assuming a parabolic profile for the density of monomers and obtained expressions for the thickness of the overlap region (OR, see Figure 1) [24–28]. These studies relate the polymerization degree N and the grafting density of chains ρ_g to the thickness of the overlap region via various scaling arguments. There is a vast literature of the computer simulations focusing on the equilibrium structure of interacting polymer brushes and confirming these scaling artuments [29–35] (also see Ref [36] for a recent review by Kreer). These studies focus on various regimes from semidilute to melt and show that two brushes indeed interdigitate one another under compression (Figure 1). These studies implicitly assume that chains can enter the OR partially (i.e. a single chain occupies the OR on average less than N monomers) and not all grafted grafted chains can be found inside the OR at any given time (as opposed to the AG model). To best of our knowledge, no study has systematically investigated statistics of chain sections inside the OR along with the fraction of chains that can coexist in the OR.

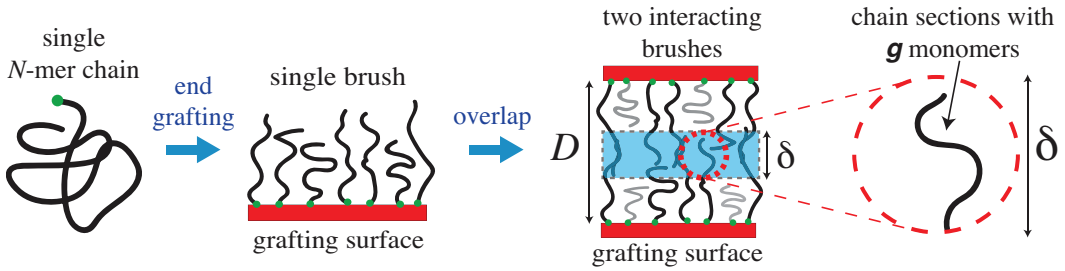

Figure 1. Illustration of formation of polymer brushes. Chains are grafted by one of their free ends onto a surface with a grafting density ρ_g. Densely grafted chains form a polymer brush. If two brushes are brought to physical contact face to face, two brushes would interact via an overlap region (OR, shaded area between the brushes) with a thickness of δ. At any instant, some chains are outside of the OR (gray chains). If a grafted chain enters the OR, it can occupy the OR with $g < N$ monomers on average. The Gaussian size of the g-mer sections determine the width of the OR.

In this study, in order to investigate the relationship between the amount of brush overlap and chain statistics inside the OR for two molten polymer brushes strongly pressed to each other as shown in Figure 1, we conduct large scale coarse-grained molecular dynamics (MD) simulations. We analyze simulation trajectories by using in-house codes and compare our results to the scaling arguments to verify their validity for a range of polymerization degrees between $N = 30, 240$ and two grafting densities ρ_g. While our MD simulations are in excellent agreement with previous theoretical arguments for nonentangled polymer brushes, they also reveal that the chain section inside the OR are indeed Gaussian, and at intermediate compression levels, only a small

fraction of grafted chains can be found inside the OR.

The rest of the paper is organized as follows. First we present an overview of the scaling arguments for the overlap region and the conformation of chain section inside the OR from the literature along with additional scaling analyses. We then summarize our simulation methodology and compare our MD-simulation results with the scaling arguments. We discuss the importance of our results together with short future perspective in the conclusion section.

2. Theoretical overview

Consider that N_{ch} linear polymer chains of N monomers each are grafted on a planar surface by one of their ends as shown in Figure 1. There is no attraction between the polymer monomers and the surface, but there is steric repulsion between them. The grafting density of the polymers is defined as $\rho_g = N_{ch}/A$, where the area of the planar surface is A. A critical grafting density is defined as $\rho_g^* \equiv 1/R_0^2$, where $R_0 = N^{1/2}b$ is the Gaussian size of a single chain. Here b is the Kuhn-segment size, in which all the chemical details of the polymer monomer is embedded. If $\rho_g < \rho_g^*$, the surface is carpeted by sparsely placed (noninteracting) chains, which is also known as mushroom regime. If $\rho_g > \rho_g^*$, the grafted chains are close enough to sterically interact with each other and stretched in the direction perpendicular to the surface (Figure 1). As a result, the grafted polymer form a brush layer composed of stretched chains. In this study, we only consider this brush regime.

If two identical polymer brushes are brought into physical contact by bringing the grafting surfaces to a surface separation of D, as shown in Figure 1, the chains of one brush diffuse through the other brush layer. The end sections of grafted chains can only interdigitate throughout the other brush up to a certain depth of δ (Figure 1). Note that only inside this overlap region (OR) the monomers of the two brushes can interact. If the separation distance between the two surfaces is small (i.e. high compression, $D \leq R_0$), there is a complete overlap between the brushes. In this case, the thickness of the OR, δ, is determined solely by the separation distance,

$$\delta = D \approx \frac{N\rho_g}{\phi} \quad \text{for} \quad D \leq R_0 \tag{1}$$

after using the expression $\phi \approx NN_{ch}/(AD) \approx N\rho_g/D$ for the number density of monomers. Here, and throughout the paper, the $\approx$ signs denote scaling relations, for which the numerical prefactors on the order of unity are dropped. When $D \leq R_0$, all N monomers of each grafted chain are found inside the OR.

For larger separations, $D > R_0$, the overlap between the two brushes is relatively less strong. This will bring the thickness of the OR to a size $\delta < D$. The equilibrium width of the OR, δ, under weak interdigitation was predicted by assuming a parabolic concentration profile as [24, 26, 40].

$$\delta \approx \left(\frac{N^2b^4}{D}\right)^{1/3} \sim N^{2/3}D^{-1/3} \quad \text{for} \quad D > R_0. \tag{2}$$

The above expression leads to $\delta = R_0$ at $D = R_0$. If $D < R_0$, the width of the OR is given by Eq. 1. If we use the expression $\phi \approx N\rho_g/D$, Eq. 2 can also be written as a function of the grafting density and N as

$$\delta \approx b\left(\frac{\phi Nb}{\rho_g}\right)^{1/3} \sim \rho_g^{-1/3}N^{1/3} \quad \text{for} \quad D > R_0, \tag{3}$$

which indicates that with increasing grafting density, the overlap between two brushes decreases.

From an experimental point of view, a relation between δ and D could more useful. By combining Eqs. 1 and 2, the width of the OR can be written as a function of the surface separation as

$$\frac{\delta}{D} \approx \begin{cases} 1 & \text{for} \quad D \leq R_0 \\ (D/R_0)^{-4/3} & \text{for} \quad D > R_0 \end{cases}, \tag{4}$$

Next, we will consider the conformation of chain sections inside the OR. A grafted chain with its one end free diffuses in and out of the OR. Yet, when $D < R_0$, a single chain is completly inside the OR since $\delta = D$. However, when $D > R_0$, only a certain number of monomers, $g < N$, is able to diffuse through the OR (see Figure 1). It is these monomers that can interact with the monomers of the opposite brush. A relation between g and δ can be established as follows: In the brush limit, grafted chains are not stretched uniformly [26]; while the chain sections near the grafting surface are highly stretched, the chain sections near the free ends are weakly stretched or not stretched at all. This implies that the elastic energy of the end section of g monomers can be assumed to be on the order of the thermal energy k_BT, where k_B is the Boltzmann constant and T is the absolute temperature. In this case, the chain segments inside the OR perform a random walk, which leads to

$$\delta \approx g^{1/2} b. \tag{5}$$

While Eq. 5 clarifies the conformation of the chain segments inside the OR, it does not provide a relationship between the macroscopic parameters of interest, namely D and N, both of which can be controlled experimentally [39]. By combining Eq. 5 with Eqs. 2 and 3, we can obtain an expression for the number of monomers per chain segment within the OR as

$$g \approx N \left(\frac{R_0}{D}\right)^{2/3} \approx \left(\frac{\phi N b}{\rho_g}\right)^{2/3} \sim \rho_g^{-2/3} N^{2/3} \quad \text{for} \quad D > R_0. \tag{6}$$

Eq. 6 leads to $g = N$ at $D = R_0$. Consequently, for any $D > R_0$, $g/N < 1$.

Eqs. 3 and 6 have some important consequences for moderate separation distances between the grafting surfaces; for $D \geq R_0$, the probability of finding a grafted chain (its free end) inside the OR is $\Psi = 1$ (i.e. Ψ is the number fraction of chain inside the OR), and thus, $g = N$ as shown above (i.e. a chain occupies the OR with all of its monomers). As the separation is increased to $D > R_0$ and the thickness of the OR decreases, at any time, some chains have to stay outside of the OR (see the gray chains in Figure 1). This, on average, leads to a $\Psi < 1$. Recall that chains constantly diffuse in and out of the OR, so individual chains inside the OR may change. Assuming a homogeneous monomer density in between the surfaces, the number of monomers inside the OR is $n \approx \delta \phi A$. In terms of Ψ, the same number can also be written as $n \approx g N_{ch} \Psi$ since each chain enters the OR with g monomers on average . Equating these two expressions of n leads to,

$$\Psi \approx \left(\frac{\phi b^2}{\delta \rho_g}\right) \approx \frac{g}{N} \quad \text{for} \quad D > R_0, \tag{7}$$

after making use of Eq. 3. Eq. 7 indicates that for $g \ll N$, not all but a small number of grafted chains can enter the OR and interact with the opposing brush. If we combine Eqs. 5 and 7, the probability of finding a chain inside the OR is

$$\Psi \approx \begin{cases} 1 & \text{for} \quad D \leq R_0 \\ (D/R_0)^{-2/3} & \text{for} \quad D > R_0 \end{cases} \tag{8}$$

indicating that the probability of finding a tagged chain inside the OR is unity when surfaces are too close and decreases below unity as the brushes are separated from each other. In the next section, we will discuss how the chain conformation and overlap between two brushes predicted by the scaling arguments above compare with MD simulations for molten brushes.

3. Molecular dynamics simulations

3.1. Simulation model

To construct computational models for our polymer brushes, we use coarse-grained (CG) Kremer–Grest bead-spring chains [41] (Figure 2). In this model, all chemical details of the polymer chains are taken care by bonded and nonbonded interaction potentials. Nonbonded steric interactions between beads are represented by a repulsive shifted-truncated Lennard–Jones (LJ) potential

$$U(r_{ij}) = \begin{cases} 4\epsilon \left[\left(\frac{\sigma}{r_{ij}}\right)^{12} - \left(\frac{\sigma}{r_{ij}}\right)^{6} + \frac{1}{4} \right] & \text{for} \quad r_{ij} < r_c \\ 0 & \text{for} \quad r_{ij} > r_c, \end{cases} \tag{9}$$

where σ is the LJ bead size, r_{ij} is the distance between ith and jth beads, the cut-off distance is $r_c = 2^{1/6}\sigma$, and the strength of the LJ potential.

In order to model covalent bonds, two beads are connected via the finite extensible nonlinear elastic (FENE) potential

$$U_{FENE}(r) = -\frac{1}{2} k r_0^2 \ln\left(1 - \frac{r^2}{r_0^2}\right) \quad \text{for} \quad r < r_0, \tag{10}$$

where r is the distance between the bonded beads, the spring constant is $k = 30\epsilon/\sigma^2$, and the maximum bond length is $r_0 = 1.5\sigma$. Eqs. 9 and 10 together provide that $b \approx 1\sigma$.

The polymer chains with $N = 30, 60, 120, 240$ beads are attached by one of their free ends onto planar surfaces with square-lattice pattern composed of fixed 40×36 beads. The vertical distance D between the two opposing plates is determined by $D = 2N\rho_g/\phi$ in order to obtain a number density of $\phi \approx 0.85\sigma^{-3}$ for grafting densities of $\rho_g = 1/9\sigma^{-2}$ and $1/4\sigma^{-2}$. The surface and the chain bead also interact via Eq. 9. but the LJ cut-off between the surface and anchored chain beads is increased to $r_c = 2 \times 2^{1/6}\sigma$ to avoid excess stretching of the tethered bonds.

The starting configurations of opposing brushes are constructed in three steps. First, two single brushes are built without physical contact as mirror images. After a short relaxation process, the top brush is brought to the prescribed interplate distance at $z = D$ while the bottom brush is fixed at $z = 0$ to obtain the desired volume fraction (Fig. 2). The overlapped brushed are relaxed for a time of minimum $4\tau_R$, where $\tau_R \simeq N^2\tau_0$ is the Rouse relaxation time for a single free linear chain in melt conditions with $\tau_0 \simeq 200$ MD steps [30].

All simulations are run using LAMMPS MD package [42]. The Verlet algorithm is employed within constant volume V and temperature T. The temperature T is kept constant at $T = 1.0\epsilon/k_B$ by using a Langevin thermostat with a damping constant $\Gamma = 0.5\tau_{LJ}^{-1}$. Periodic boundary conditions are introduced in lateral, i.e. $\hat{x}$ and $\hat{y}$, directions. Simulations are run with a time step of $\Delta t = 0.005\tau_{LJ}$. Here $\tau_{LJ} = \sigma\sqrt{m/\epsilon} \simeq \tau_0$ represents the LJ time unit, where LJ mass m is set to unity for all monomers.

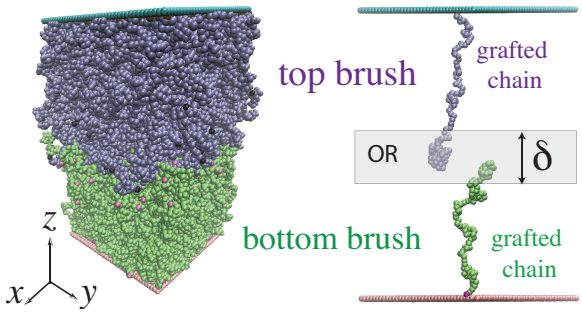

Figure 2. Left panel shows the perspective view of a simulation box with dimensions $40 \times 36 \times 120\sigma^3$ for $N = 120$ and $\rho_g = 1/4\sigma^{-2}$. Different colors are used to indicate top and bottom brushes, otherwise both brushes are identical. Right panel shows two arbitrary selected chains from each brush. The gray shaded area shows the overlap region (OR). The snapshots are obtained with VMD [43].

3.2. Comparison of MD results with scaling theories

In order to directly compare our course-grained simulations to the scaling expressions, the main challenge is to extract the thickness of OR for our brush systems with various N and ρ_g parameters. To achieve this, we make use of the monomer concentration profiles of the top $\rho_{top}(z)$ and bottom $\rho_{bott}(z)$ brushes in the $\hat{z}$ direction (Figure 3). The two concentration profiles overlap in the middle of the surfaces (i.e. $z = D/2$), around which the beads of both brushes interact. Accordingly, the thickness of the overlap region could be numerically calculated from MD trajectories via

$$\delta \equiv 2\left[\int_0^D z'^2\omega(z)dz - \left(\int_0^D z\omega(z)dz\right)^2\right], \tag{11}$$

where we define the cross product of the two concentrations as $\omega(z) \equiv \rho_{top}(z)\rho_{bott}(z)$ [37]. In Figure 3, we show a representative case of the density profiles for two pressed brushes with $N = 60$ and $\rho_g = 1/4\sigma^{-2}$. A density peak (red curve) indicates the OR, in which two brushes can interact sterically via their chain sections.

In Figure 4, the thickness of OR, δ, is shown for various chain sizes and grafting densities. For each case, the values of g are calculated by counting the monomers of a grafted chain if the z-coordinate of its terminal monomer is within the OR as illustrated in Figure 2. The data in Figure 4 indicate that the size of the chain sections within the OR can be described by our scaling expression in Eq. 5 within the error bars, which confirms that chain sections obey the Gaussian statistics. Particularly, the average end-to-end distance of the chain segments with g monomers, r_{ee}, follows the random walk statistics (i.e. $r_{ee} \sim g^{1/2}$). Thus, the thickness of the OR zone is related to the characteristic size of the chain section in the OR (i.e. $r_{ee} \approx \delta$). Note that for larger values of g, the scaling prediction desribes the data more accurately since the scaling models are ideally for the thermodynamic limit of long chains.

Figure 5 shows the OR thickness rescaled by the interplate distance and the grafting density according to Eqs. 2 and 3, respectively, as a function of polymerization degree of the grafted brushes, N. In Figure 5, the data for two different grafting densities overlap well within the error tolerance (the size of the error bars is roughly the size of the markers) indicating that both system are in the brush regime. The scaling relations in Eqs. 2 and 3 describe the data well (dotted lines in the figure) particularly for brushes composed of long chains (i.e. $N > 60$). We attribute the discrepancy between simulations and theory for short chains to the smaller

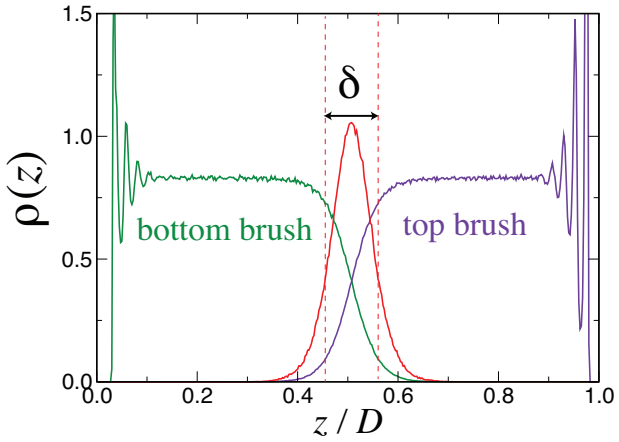

Figure 3. The monomeric density profiles of bottom and top brushes for two interacting brushes each with $N = 60$ and $\rho_g = 1/4\sigma^{-2}$ as a function of the rescaled intersurface distance z/D. The red curve is the cross product of the two density profiles and amplified by a factor of 8 to guide the eye. The width of the cross-product corresponds to the thickness of the overlap region (OR) via Eq. 11.

number of beads per chain wihin OR. In addition, since the height of a single brushes scales as $H \sim N\sigma_g^{1/2}$, it is possible that the free ends of the chain interact with the opposing plate in the brushes of short chains (i.e. $H \approx D$). These interactions in turn can distort the random walks of the segments in the OR.

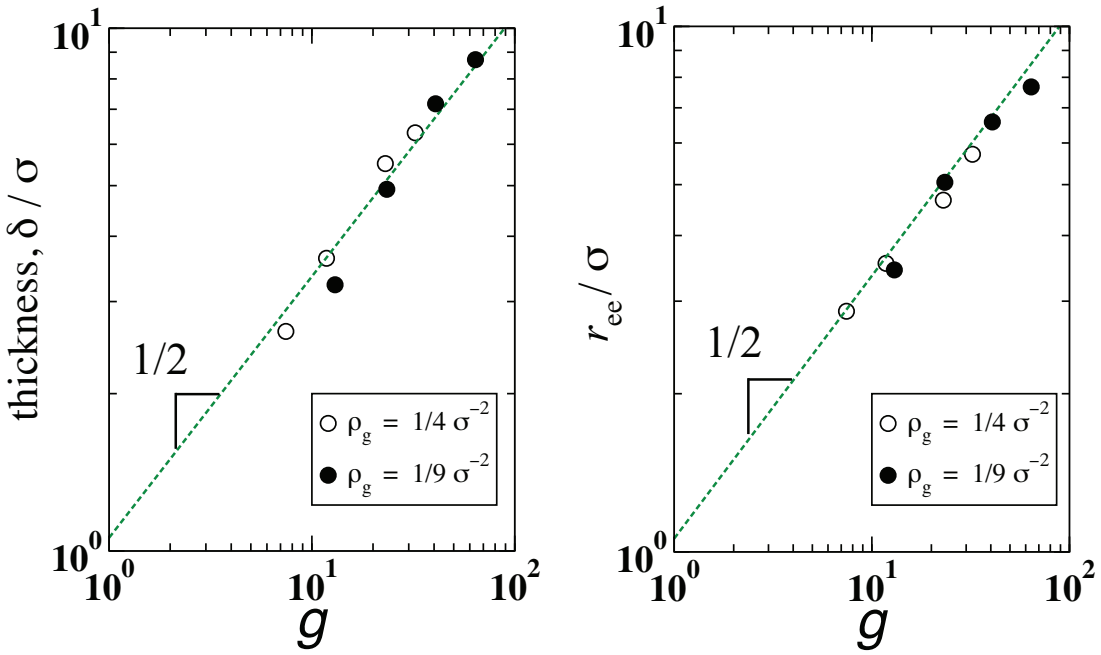

Figure 4. Left panel: the thickness of the OR for various brush systems for two different grafting densities. Right panel: the average end-to-end size of the chain section within the OR as a function of the average number of Kuhn segments per chain in the OR (refer to Figure 1). The dashed lines have the slopes of 0.5 from Eq. 5.

To reveal the change in δ as two brushes approach each other, we plot the thickness of the OR rescaled

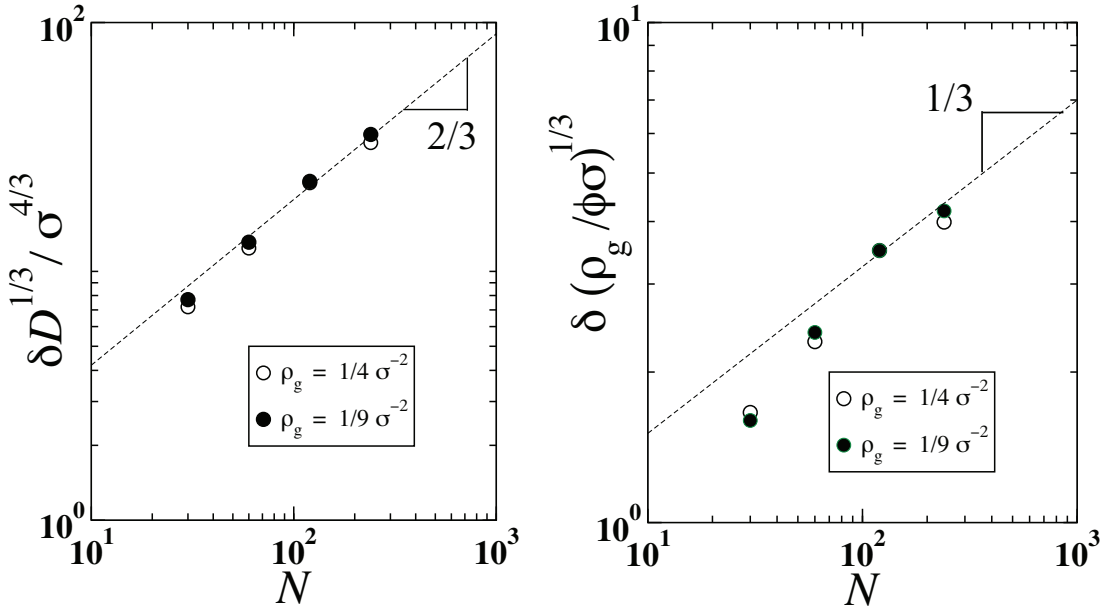

Figure 5. Left panel: the thickness of the OR scaled by the cubic root of the interplate distance is shown as a function of polymerization degree for two different grafting densities. The dashed line has the slope from Eq. 2. Right panel: the thickness of OR rescaled by the grafting density. The dashed line has the slope from Eq. 3.

by interplate distance D as a function of D/R_0. Note that each system has its own D and R_0 values (Table 1) since for various brushes with different values of ρ_g and N, the surface separation D is set to obtain a number density of $\phi = 0.85\sigma^{-3}$. Figure 6 shows that the thickness of OR increases as the surfaces are brought closer in accord with Eq. 4. At very strong compression, we expect $\delta \to D$. Since our brush system are within the regime of $D > R_0$, they only capture the regime in which OR increases with compression but does not reach the limit of $\delta = D$. If we fit the data points with a function $f(x) \sim x^{\alpha}$, we obtain $\alpha \approx -1.4$, which is in good agreement with the exponent of –4/3 given in Eq. 4.

Table . Summary of parameters and findings for various brush system used in this study. The number of Kuhn segments per grafted chain N, grafting density ρ_g, interplate distance D,the thickness of OR δ, the number of Kuhn segments per chain g in the OR (with free end inside the overlap region), and the probability of finding a chain in OR, Ψ, whose at least its free end is in the OR.

N	ρ_g $[\sigma^{-2}]$	$D[\sigma]$	$\delta[\sigma]$	g	Ψ
30	0.11	11	3.2	13	0.64
30	0.25	21	2.6	7.4	0.44
60	0.11	19	4.9	23	0.55
60	0.25	40	3.6	12	0.38
120	0.11	35	7.2	41	0.50
120	0.25	71	5.1	23	0.33
240	0.11	68	8.7	64	0.38
240	0.25	143	6.3	32	0.26

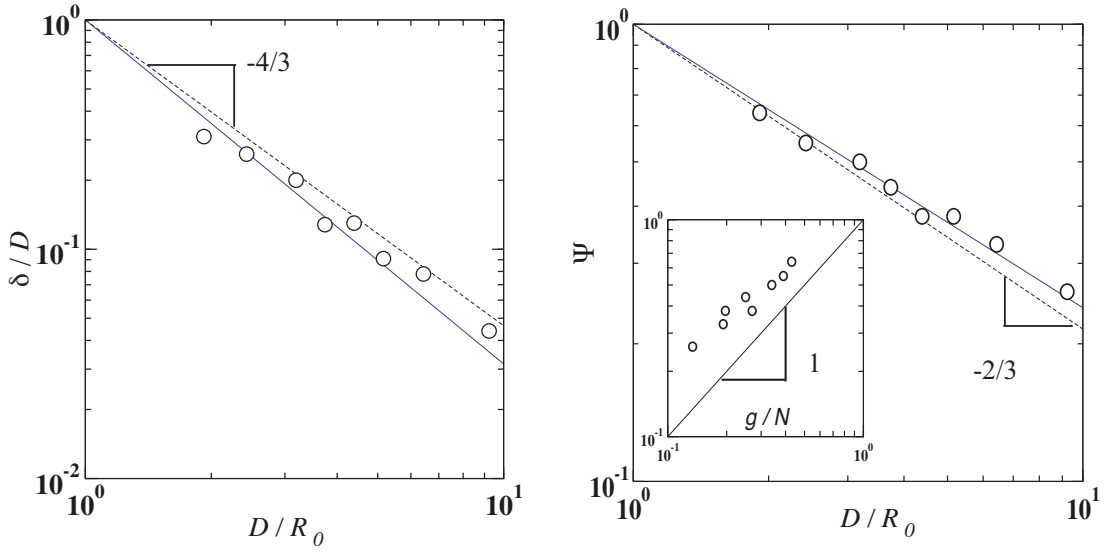

Figure 6. Left panel: The width of the OR rescaled by the interplate distance as a function of the interplate distance rescaled by the Gaussian size of the free chains with N monomers for all brushes. The dashed line is the slope of –4/3 from Eq. 3. Right panel: The fraction of chains entering the OR with their free ends as a function of the interplate distance rescaled by the Gaussian size of the free chains with N monomers for all brushes. This approach ignores the loops but ensures that the end sections of the chains, which determines δ, are inside the OR. The dashed line has the slope of –2/3 from Eq. 8, and the solid line is a fit with a slope of –0.63. Inset shows the same fraction but as a function of monomer per chain within the OR. The line has the slope of unity (Eq. 7).

Next, by using our simulation trajectories, we calculate the probability of finding a chain within the OR region, Ψ. To calculate this parameter, we accept a rule to determine any chain inside the OR. Accordingly, if the end monomer of a chain is inside the OR at a given time step, then we count this chain "in the OR". We do not count loops unless the end monomer is outside of the OR. We show our results in Figure 6 for various N and ρ_g values. The scaling prediction in Eq. 8 describes the data well, indicating the participation of chains with increasing compression (or decreasing D). In the inset of Figure 6, we also show the same data but as a function of g/N; As $g \to N$, indeed $\Psi \to 1$ as predicted in Eq. 7, since all chains would be in the OR at $D \leq R_0$.

Overall, the scaling theories and equilibrium MD simulations of polymer brushes are in well agreement, particularly if the grafted chains are long. Deviation for short grafted chains arise due to finite size effects and increasing confinement of the chains between the surfaces.

4. Conclusion

In this work, using MD simulations and scaling arguments, we study the equilibrium properties of two identical molten polymer brushes strongly compressed to each other. We demonstrate that the size of the overlap region, through which the end sections of the grafted chains interdigitate and two polymer brushes intact, increases as the grafting surfaces are brought closer. In parallel, more chains enter this region as the surfaces are pressed closer (otherwise on average only finite number of chains is found in the overlap region). Since the interplate distance is a controllable experimental parameter, along with the polymerization degree, our results could be used to determine the grafting density of brushes by the surface force apparatus (SFA) [39]. Additionally, in the self-assembly of polymer-grafted colloids, the interaction between grafted polymers, thus the amount of

overlap, could change the phase behavior [44, 45]. In that sense, by controlling density of colloids, c, hence, the interplate distance (i.e. $D \sim c^{-1/3}$), one can change the average interaction strength between the colloids, thus, the final phases. Further, our study could provide insights into medical applications, design of artificial joints, and industrial lubricants with low friction.

There are several issues that we have not considered in this study but can affect the interactions between two brushes. First of them is the polydispersity. While here we only consider the overlapping brushes of identical chains, the polydispersity will be encountered in the synthesis of polymer brushes in practice. In polydisperse brushes, we indeed expect certain changes in the conformations of grafted polymers; The field-theoretical calculations predicted that in a highly-polydisperse brush, while short chains stay compressed near the surface (constrained by longer ones), longer chains can adapt a " flower-stem" configuration, where the chain sections near the surface are more stretched as compared to the section near the free ends [46]. As a result, the polydispersity can be expected to decrease the number fraction of chains in the OR and increase the thickness of the OR by promoting brush-brush interdigitation [47]. Further, the recent theoretical calculations predict that excessive polydispersity can significantly change the density profile of brushes and even lead to an increase in the OR thickness as the compressed brushes are separated [48]. Nevertheless, the experimentally observed interaction energies between the two brushes are qualitatively well described by equilibrium theories, at least for values of polydispersity index around unity [35]. Along with the polydispersity, brushes with no ends, such as those composed of ring polymers, could also affect the amount of interdigitation between overlapping brushes [37] in a grafted-density and polymerization-degree dependent way. Lastly, in the situations where the polymer-coated surfaces move relative to each other at shear rates comparable or higher than the chain relaxation times, the width of the OR and all the related parameters would change in a shear-rate dependent manner [37, 38]. This dependence can be quite different for entangled polymers. We plan to challenge some of these questions in our future studies.

Acknowledgment

The author acknowledges anonymous referees for their individual assessments, specifically for bringing the effects of polydispersity to his attention. This research was supported by the Scientific and Technological Research Council of Turkey (TÜBİTAK) 2232 Program (2018/4) under the project ID 119C010.

References

[1] Binder K, Kreer T, Milchev A. Polymer brushes under flow and in other out-of-equilibrium conditions. Soft Matter 2011; 7: 7159.

[2] Matyjaszewski K, Miller PJ, Shukla N, Immaraporn B, Gelman A et al. Polymers at interfaces: using atom transfer radical polymerization in the controlled growth of homopolymers and block copolymers from silicon surfaces in the absence of untethered sacrificial initiator. Macromolecules 1999; 8716-8724.

[3] Hawker C, Bosman A, Harth E. New polymer synthesis by nitroxide mediated living radical polymerizations. Chemical Reviews 2001; 101 (12): 3661-3688.

[4] Advincula R, Brittain WJ, Caster KC, Rühe JE. Polymer Brushes: Synthesis, Characterization, Applications. Weinheim, Germany: VCH- Wiley, 2004.

[5] Azzaroni O. Polymer brushes here, there, and everywhere: recent advances in their practical applications and emerging opportunities in multiple research fields. Journal of Polymer Science Part A: Polymer Chemistry 2012: 3225-3258.

[6] Wei-Liang C, Cordero R, Tran H, Ober C. 50th anniversary perspective: polymer brushes: novel surfaces for future materials. Macromolecules 2017; 50: 4089-4113.

[7] Motornov M. Stimuli-responsive colloidal systems from mixed brush-coated nanoparticles. Advanced Functional Materials 2007; 17: 2307-2314.

[8] Pincus P. Colloid stabilization with grafted polyelectrolytes. Macromolecules 1991; 24 : 2912-2919.

[9] Groll J, Fiedler J, Bruellhoff K, Moeller M, Brenner RE. Novel surface coatings modulating eukaryotic cell adhesion and preventing implant infection. The International Journal of Artificial Organs 2009; 32 (9).

[10] Akiba U, Anzai J. Recent progress in electrochemical biosensors for glycoproteins. Sensors 2016; 16 (12): 2045.

[11] Zhou F, Huck WTS. Surface grafted polymer brushes as ideal building blocks for smart surfaces. Physical Chemistry Chemical Physics 2006; 8: 3815.

[12] Gandhi A, Paul A, Sen SO, Sen KK. Studies on thermoresponsive polymers: phase behaviour, drug delivery and biomedical applications. Asian Journal of Pharmaceutical Sciences 2015; 10 (2): 99-107.

[13] Bajpai AK, Shukla SK, Bhanu SKS. Responsive polymers in controlled drug delivery. Progress in Polymer Science 2008; 33: 1088-1118.

[14] Kwon OH, Kikuchi A, Yamato M, Okano T. Accelerated cell sheet recovery cografting of PEG with PIPAAm onto porous cell culture membranes, Biomaterials 2003; 24: 1223-1232.

[15] Kumar S, Dory YL, Lepage M, Zhao Y. Surface-grafted stimuli-responsive block copolymer brushes for the thermo-, photo- and ph-sensitive release of dye molecules. Macromolecules 2011; 44 (8): 7385-7393.

[16] Sally LG. Intelligent control of surface hydrophobicity. ChemPhysChem 2007; 8 (14): 2036-2050.

[17] Klein J. Shear, friction, and lubrication forces between polymer-bearing surfaces. Annual Review of Materials Science 1996; 26: 581-612.

[18] Sterner OR. Reducing friction in the eye: a comparative study of lubrication by surface-anchored synthetic and natural ocular mucin analogues. ACS Applied Materials & Interfaces 2017; 9: 20150-20160.

[19] Lee S. Sticky and slippery: interfacial forces of mucin and mucus gels. In: Aqueous Lubrication: Natural and Biomimetic Approaches. Singapore: World Scientific Publishing Co. Pte. Ltd., 2014.

[20] Coles JM, Chang DP, Zauscher S. Molecular mechanisms of aqueous boundary lubrication by mucinous glycoproteins. Current Opinion in Colloid & Interface Science 2010; 15: 406-416.

[21] Klein J. Repair or replacement: a joint perspective. Science 2009: 47-48.

[22] De Gennes PG. Ibid. Journal de Physique 1976 (37): 1443 (in French).

[23] Alexander S. Adsorption of chain molecules with a polar head a scaling description. Journal de Physique 1977; 38: 983-987 (in French with an abstract in English).

[24] Milner S, Witten T, Cates M. Theory of the grafted polymer brush. Macromolecules 1988; 21 (8): 2610-2619.

[25] Skvortsov AM, Pavlushkov IV, Gorbunov AA, Zhulina YB, Borisov OV et al. Structure of densely grafted polymeric monolayers. Polymer Science U.S.S.R. 1988; 30 (8): 1706-1715.

[26] Milner S, Witten T, Cates M. A parabolic density profile for grafted polymers. Europhysics Letters 1988; 5 (5): 413-418.

[27] Witten T, Leibler L, Pincus P. Stress relaxation in the lamellar copolymer mesophase. Macromolecules 1990; 23: 824-829.

[28] Amoskov VM, Birshtein TM, Pryamitsyn VA. Theory of liquid-crystalline (LC) polymer brushes: interpenetrating brushes. Macromolecules 1998; 31 (11): 3720-3730.

[29] Erbaş A, Rubinstein M. Viscous friction of polymer brushes. In: APS March Meeting; Baltimore, MD, USA; 2013.

[30] Murat M, Grest GS. Interaction between grafted polymeric brushes: a molecular-dynamics study. Physical Review Letters 1989; 63: 1074-1077.

[31] Liberelle B, Giasson S. Friction and normal interaction forces between irreversibly attached weakly charged polymer brushes. Langmuir 2008; 24 (4): 1550-1559.

[32] Binder K, Kreer T, Milchev A. Polymer brushes under flow and in other out-of-equilibrium conditions. Soft Matter 2011; 7 (16): 7159.

[33] Binder K, Milchev A. Polymer brushes on flat and curved surfaces: how computer simulations can help to test theories and to interpret experiments. Journal of Polymer Science Part B: Polymer Physics 2012; 50 (22): 1515-1555.

[34] Kreer T, Balko SM. Scaling theory for compressed polymer-brush bilayers. ACS Macro Letters 2013; 2: 944-947.

[35] Desai PR, Sinha S, Das S. Compression of polymer brushes in the weak interpenetration regime: scaling theory and molecular dynamics simulations. Soft Matter 2017; 13: 4159-4166.

[36] Kreer T. Polymer-brush lubrication: a review of recent theoretical advances. Soft Matter 2016; 12: 3479-3501.

[37] Erbaş A, Paturej J. Friction between ring polymer brushes. Soft Matter 2015: 1-10.

[38] Galuschko A, Spirin L, Kreer T, Johner A, Pastorino C et al. Frictional forces between strongly compressed, nonentangled polymer brushes: molecular dynamics simulations and scaling theory. Langmuir 2010; 26 (9): 6418-6429.

[39] Tadmor R, Janik J, Klein J, Fetters LJ. Sliding friction with polymer brushes. physical Review Letters 2003; 91: 115503.

[40] Zhulina EB, Borisov OV, Pryamitsyn VA, Birshtein TM. Coil-globule type transitions in polymers. 1. Collapse of layers of grafted polymer chains. Macromolecules 1991;24 (1): 140-149.

[41] Kremer K , Grest GS. Dynamics of entangled linear polymer melts: a molecular-dynamics simulation. The Journal of Chemical Physics 1990; 92 (8): 5057.

[42] Plimpton S. Fast Parallel Algorithms for Short-Range Molecular Dynamics. Journal of Computational Physics 1995;17: 1-19.

[43] Humphrey W, Dalke A, Schulten K. VMD - Visual Molecular Dynamics. Journal of Molecular Graphics 1996; 14 (1): 33-38.

[44] Seo SE, Girard M, De La Cruz MO, Mirkin CA. Non-equilibrium anisotropic colloidal single crystal growth with DNA. Nature Communications 2018; 9 (1): 1-8.

[45] Wijmans CM, Zhulina EB. Polymer brushes at curved surfaces. Macromolecules 2015; 26: 1-11.

[46] De Vos WM, Leermakers FAM. Modeling the structure of a polydisperse polymer brush. Polymer 2009; 50 (1): 305-316.

[47] Milner ST, Witten TA, Cates ME. Effects of polydispersity in the end-grafted polymer brush. Macromolecules 1989; 22: 853-861.

[48] Klushin LI, Skvortsov AM, Qi S, Kreer T, Schmid F. Polydispersity effects on interpenetration in compressed brushes. Macromolecules 2019; 52 (4): 1810-1820.